NJC

PAPER

View Article Online
View Journal

Cite this: DOI: 10.1039/c6nj00833j

Mononuclear heteroleptic complexes of copper(I) with 5-phenyl-2,2′-bipyridine and triphenylphosphine: crystal structures, Hirshfeld surface analysis and luminescence properties†‡

Damir A. Safin,[a] Christophe M. L. Vande Velde,[b] Maria G. Babashkina,*[a] Koen Robeyns[a] and Yaroslav Filinchuk[a]

Received (in Victoria, Australia) 15th March 2016,
Accepted 5th May 2016

DOI: 10.1039/c6nj00833j

www.rsc.org/njc

The reaction of 5-phenyl-2,2′-bipyridine (**L**) with a mixture of CuCl or CuBr and PPh_3 leads to the formation of mononuclear heteroleptic complexes [CuL(PPh_3)Cl] (**1**) and [CuL(PPh_3)Br] (**2**). According to X-ray diffraction, **1** and **2** crystallize in the triclinic $P\bar{1}$ and orthorhombic *Pbca* space groups, respectively. The structure of **1** contains four independent molecules in the asymmetric unit. Both structures reveal that each tetracoordinated copper(I) atom is linked to the two nitrogen atoms of **L**, one halogen and one PPh_3 with the formation of a slightly distorted trigonal pyramidal coordination core. Both structures are additionally stabilized by weak intramolecular π···π stacking interactions formed between the terminal pyridine fragments of two ligands **L** corresponding to two adjacent molecules. Hirshfeld surface analysis showed that the structures of both complexes are highly dominated by H···H and H···C contacts and also characterized by H···Hal, C···C, H···N and C···N contacts. Both **1** and **2** were found to be emissive in the solid state at 298 K, with maxima at 596 and 610 nm, respectively, due to a (M + Hal)LCT excited state. The observed blue-shifting of the emission maximum of **1** and **2** compared to that of the previously reported [CuL(PPh_3)I] can be explained by the replacement of the iodide by a weaker electron-donating bromide and chloride, respectively, lowering the HOMO energy level, less influencing the LUMO energy, and thus resulting in an increase of the HOMO–LUMO energy gap. This explanation is further supported by comparison with the recently reported emission maxima at 630 and 575 nm of the closely related complexes, namely [CuL(PPh_3)I] and [CuL(PPh_3)$_2$]BF_4, respectively. The emission maxima of **1**, **2** and [CuL(PPh_3)I] are slightly (12–16 nm) shifted to longer wavelengths when the temperature was lowered to 77 K.

Introduction

Emissive transition-metal complexes are of ever increasing interest due to their potential application in organic light-emitting devices (OLEDs), light-emitting electrochemical cells (LECs), chemical sensors/probes and biological labeling.[1] Copper(I)-containing complexes have become an important class of luminophores because of their relative abundance, low cost, attractive photophysical properties, electroluminescence, and solar energy conversion.[2] In this context, the phosphine-containing copper(I) complexes seem to be the most widely studied, among which heteroleptic complexes with pyridine-containing ligands have attracted recent interest.[2]

N-heterocyclic ligands, in particular polypyridine compounds, are known to be efficient tools to tune the luminescence properties of copper(I) complexes.[3] These ligands can be easily modified by introducing different substituents, imposing a variety of electronic, steric and conformational effects on both the coordinated chelate and coordination core. Furthermore, the nature of additional ligands, in particular halides and phosphines, was found to affect the luminescence properties of copper(I) compounds.[4]

N-heterocyclic compounds such as 2,2′-bipyridine, 1,10-phenanthroline and 2,2′:6′,2″-terpyridine seem to be the most widely used polypyridine luminophore ligands for metal complexes as well as building units in coordination and supramolecular chemistry. In particular, these compounds are known to be efficient ligands for dye-sensitized solar cells.[5] Furthermore, the renaissance of a highly attractive ligand,

[a] Institute of Condensed Matter and Nanosciences, Molecules, Solids and Reactivity (IMCN/MOST), Université catholique de Louvain, Place L. Pasteur 1, 1348 Louvain-la-Neuve, Belgium. E-mail: maria.babashkina@gmail.com
[b] Faculty of Applied Engineering, Advanced Reactor Technology, University of Antwerp, Salesianenlaan 90, BE-2660 Hoboken, Belgium

† Dedicated to Professor Wolfgang Kaim on the occasion of his 65th Birthday.

‡ CCDC 1452072 (**1**) and 1452073 (**2**). For crystallographic data in CIF or other electronic format see DOI: 10.1039/c6nj00833j

owing to the presence of three fused terpyridine-like coordination pockets, 2,4,6-tris(2-pyrimidyl)-1,3,5-triazine has recently been announced.[6] Although 2,4,6-tris(2-pyrimidyl)-1,3,5-triazine has been known for almost 60 years,[7] its coordination chemistry remains vastly underexplored. Indeed, until recently only two coordination compounds of 2,4,6-tris(2-pyrimidyl)-1,3,5-triazine were known in the literature.[8] However, during the last two years the number of reported complexes built from 2,4,6-tris(2-pyrimidyl)-1,3,5-triazine has quadrupled.[9]

By themselves, the aforementioned ligands exhibit an undesirable luminescence at short wavelengths due to the emission from the n–π* excited state.[10] Furthermore, since the 2,2'-bipyridine framework is polarized along the 5,5'-axis,[11] the introduction of aromatic substituents into these positions leads to an increase of the conjugation and, thus, an increase of polarization along this axis. This, in turn, will lead to higher luminescence as well as to a red-shift of the emission maximum.[12] With this in mind, we have recently directed our attention to 5-phenyl-2,2'-bipyridine (**L**),[13] which was synthesized according to the known procedure.[14] It was established that the reaction of **L** with a mixture of CuI or $[Cu(CH_3CN)_4]BF_4$ and PPh_3 leads to the mononuclear heteroleptic complexes $[CuL(PPh_3)I]$ and $[CuL(PPh_3)_2]BF_4$, respectively. According to diffuse reflectance spectroscopy in the solid state, free **L** exhibits bands exclusively in the UV region, while the spectra of $[CuL(PPh_3)I]$ and $[CuL(PPh_3)_2]BF_4$ also contain bands in the visible range up to about 500 and 600 nm. All three compounds were found to be emissive in the solid state. DFT calculations have shown that, while emission of **L** is due to the ligand-centered π → π* transition, luminescence of $[CuL(PPh_3)I]$ and $[CuL(PPh_3)_2]BF_4$ is attributed to (M + Hal)LCT and MLCT excited states, respectively.

In this contribution, we continue our comprehensive research into the complexation properties of **L** towards copper(I). We describe the synthesis and complete structural investigation of the mononuclear heteroleptic copper(I) complexes $[CuL(PPh_3)Hal]$ (Hal = Cl^-, **1**; Br^-, **2**) as well as their solid state luminescence properties in comparison to those of $[CuL(PPh_3)I]$ and $[CuL(PPh_3)_2]BF_4$.[13] To assess and discuss the contribution and influence of the intermolecular interactions, responsible for the crystal packing, Hirshfeld surface analysis[15] was performed and the associated 2D fingerprint plots,[16] obtained using the CrystalExplorer 3.1 software,[17] as well as the enrichment ratios,[18] derived as the decomposition of the crystal contact surface between pairs of interacting chemical species, have been calculated.

Results and discussion

The complexes **1** and **2** were prepared by reacting CuHal (Hal = Cl^-, Br^-) with two equivalents of PPh_3, followed by the addition of one equivalent of **L** (Scheme 1).[13] The obtained orange solid materials are soluble in most polar solvents.

The $^{31}P\{^1H\}$ NMR spectra of **1** and **2** in DMSO-d_6 each exhibit a unique sharp (FWHM = 5.4 Hz) signal at 25.8 and 25.9 ppm, respectively. The resonances in both spectra show a downfield shift relative to free PPh_3, supporting the fact that the

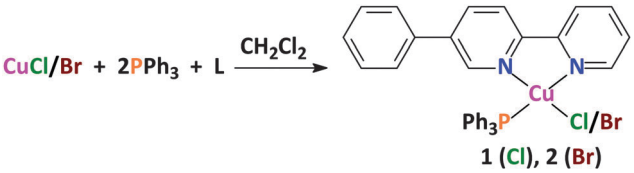

Scheme 1 Synthesis of **1** and **2**.

phosphorus atom coordinates with the metal ion. In contrast to the $^{31}P\{^1H\}$ NMR spectra, exclusively exhibiting a unique sharp signal, the ^1H NMR spectra of both complexes contain two significantly broadened singlets at 7.97–9.13 and 10.51–11.58 ppm, arising from the seven protons of the ligand **L**. This can be explained by a slow, in the NMR timescale, equilibrium in DMSO-d_6 between the coordinated and non-coordinated **L** in the structure of complexes. The signals for the PPh_3 and the remaining five protons of **L** were observed as two multiplets from 7.26 to 7.81 ppm.

According to the X-ray data, **1** and **2** crystallize in the triclinic space group $P\bar{1}$ and orthorhombic space group *Pbca*, respectively, and each comprises a discrete neutral molecule (Fig. 1). The asymmetric unit of **1** contains four independent molecules, namely **1-I**, **1-II**, **1-III** and **1-IV**. In both structures the copper(I) atom is linked to the two nitrogen atoms of **L**, one halogen and one PPh_3 affording a tetracoordinate environment. The coordination polyhedron adopted by this environment is characterized using a τ_4-descriptor for four coordinated ions.[19] The distortion index is defined as $\tau_4 = (360 - \alpha - \beta)/141$, where α and β are the two largest bond angles around the metal ion. For perfect tetrahedral, trigonal pyramid, seesaw and square planar geometries, the τ_4 values are 1.00, 0.85, 0.64–0.07 and 0.00, respectively. The τ_4 values of **1-I**, **1-II**, **1-III**, **1-IV** and **2** are 0.8665, 0.8411, 0.8748, 0.8387 and 0.8655, respectively, and indicate that the coordination geometry around Cu^I is best described as a slightly distorted trigonal pyramid. This distortion from a perfect tetrahedral environment is due to the small bite angle of **L** (Table 1). The dihedral angles between the N–Cu–N plane and the P–Cu–Hal plane are almost perpendicular and of 89.7, 87.3, 89.9, 84.0 and 87.2° for **1-I**, **1-II**, **1-III**, **1-IV** and **2**, respectively.

The two pyridine moieties of **L** are almost in the same plane for both structures, which is reflected in the dihedral angles ranging from 4.9(3) to 11.89(16)° between the two rings (Table 1). However, the phenyl fragments deviate significantly from the pyridine planes (Fig. 1 and Table 1).

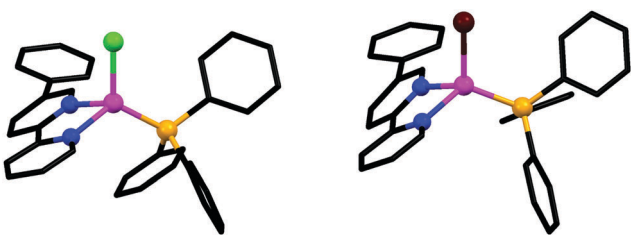

Fig. 1 Molecular structures of **1** (left) and **2** (right). Hydrogen atoms were omitted for clarity. Colour code: C = black, N = blue, Cl = green, I = purple, P = orange, Cu = magenta.

Table 1 Selected bond lengths (Å) and angles (°) for **1-I**, **1-II**, **1-III**, **1-IV** and **2**

	1-I	1-II	1-III	1-IV	2
Bond lengths					
Cu–N	2.060(5)	2.083(4)	2.072(5)	2.084(5)	2.085(3)
	2.090(4)	2.083(5)	2.102(6)	2.095(4)	2.112(3)
Cu–P	2.1719(15)	2.1897(16)	2.1823(15)	2.1933(16)	2.2047(10)
Cu–Hal	2.2809(18)	2.2765(18)	2.2798(18)	2.2774(18)	2.4405(5)
Bond angles					
N–Cu–N	78.9(2)	78.9(2)	78.6(2)	78.2(2)	79.05(11)
N–Cu–P	114.76(11)	110.13(11)	113.23(12)	109.67(11)	116.94(8)
	123.07(12)	119.57(12)	120.78(12)	122.07(12)	121.02(8)
N–Cu–Hal	108.98(13)	108.11(13)	109.53(13)	108.21(14)	108.80(8)
	114.31(14)	109.45(14)	115.88(13)	111.37(12)	111.51(8)
P–Cu–Hal	111.98(7)	121.84(7)	113.37(6)	119.67(7)	114.59(3)
Dihedral angles					
Py···Py	4.9(3)	8.8(3)	5.0(3)	8.5(3)	11.89(16)
Py···Ph(L)	32.7(3)	27.3(3)	33.8(3)	26.2(3)	18.76(17)
	37.2(3)	36.1(3)	38.2(3)	34.7(3)	29.91(17)

The Cu–N and Cu–P bond lengths in **1** and **2** are 2.06–2.11 and 2.17–2.20 Å, respectively (Table 1). The Cu–Cl bonds in **1** are about 2.28 Å, while the Cu–Br bond in **2** is about 2.44 Å. The N–Cu–N angles are identical for both complexes and about 79°, while the N–Cu–P, N–Cu–Hal and P–Cu–Hal angles vary from 109.67(11) to 123.07(12)°, from 108.11(13) to 115.88(13)° and from 111.98(7) to 121.84(7)°, respectively (Table 1).

Notably, three independent molecules of **1** as well as the molecule of the previously reported [CuL(PPh$_3$)I][13] are each stabilised by intramolecular C–H···Cu interactions, formed by one of the *ortho*-H atoms of one of the phenyl rings of PPh$_3$. The same intramolecular interactions were also observed in the structure of [CuL(PPh$_3$)$_2$]BF$_4$ but arising from two *ortho*-H atoms of two phenyl rings of two PPh$_3$.[13] These interactions are characterised by the following parameters: d(Cu···H) = 2.9–3.0 Å and ∠(C–H···Cu) = 114–121°. Three forms of C–H···M interactions, namely: hydrogen bond, agostic and anagostic were reported.[20] Hydrogen bonds comprise 3-centre–4-electron interactions with an almost linear geometry. Agostic interactions are 3-centre–2-electron interactions and characterized by the short M···H distance (1.8–2.2 Å) and C–H···M bond angles (90–130°). Anagostic interactions are largely electrostatic in nature and characterized by the long M···H distance (2.3–3.0 Å) and large C–H···M bond angles (110–170°). The observed C–H···Cu parameters in the structures of **1**, [CuL(PPh$_3$)I] and [CuL(PPh$_3$)$_2$]BF$_4$ fit those for the weak anagostic interactions.

Both structures **1** and **2** are additionally stabilized by weak intermolecular parallel displaced π···π stacking interactions with an interplanar separation of about 3.8–4.0 Å (Table 2), formed between the terminal pyridine fragments of two ligands **L** corresponding to two adjacent complexes.

A closer inspection of both crystal structures revealed no classical hydrogen bonds but further H···X short contacts. However, based on established criteria[21] these weak interactions are not directing the crystal packing or molecular structure.

Bulk samples of **1** and **2** were studied by means of X-ray powder diffraction analysis (Fig. 2). The experimental X-ray

Table 2 π···π distances (Å) and angles (°) for **1** and **2**[a]

	Cg(*I*)	Cg(*J*)	d[Cg(*I*)–Cg(*J*)]	α	β	γ
1[b]	Cg(2)	Cg(9)$^{\#1}$	3.999(3)	2.5(3)	32.5	32.3
	Cg(16)	Cg(17)$^{\#2}$	3.961(3)	5.0(3)	29.7	31.2
	Cg(23)	Cg(23)$^{\#3}$	3.779(3)	0	27.5	27.5
2[c]	Cg(2)	Cg(2)$^{\#1}$	3.784(2)	0	22.7	22.7

[a] Cg(*I*)–Cg(*J*): distance between ring centroids; α: dihedral angle between planes Cg(*I*) and Cg(*J*); β: angle Cg(*I*) → Cg(*J*) vector and normal to plane *I*; γ: angle Cg(*I*) → Cg(*J*) vector and normal to plane *J*. [b] Symmetry transformations used to generate equivalent atoms: #1 x, $1+y$, z; #2 $2-x$, $1-y$, $1-z$; #3 $1-x$, $1-y$, $1-z$. Cg(2): N(22)–C(23)–C(24)–C(25)–C(26)–C(27); Cg(9): N(142)–C(143)–C(144)–C(145)–C(146)–C(147); Cg(16): N(62)–C(63)–C(64)–C(65)–C(66)–C(67); Cg(17): N(69)–C(68)–C(70)–C(71)–C(72)–C(73); Cg(23): N(102)–C(103)–C(104)–C(105)–C(106)–C(107). [c] Symmetry transformations used to generate equivalent atoms: #1 $1-x$, $2-y$, $1-z$. Cg(2): N(22)–C(23)–C(24)–C(25)–C(26)–C(27).

powder patterns are in agreement with the calculated powder patterns obtained from the single crystal X-ray analyses, showing that the bulk materials **1** and **2** are free from phase impurities.

In order to examine the interactions in the crystal structures of **1** and **2**, the Hirshfeld surface analysis[15] and the 2D fingerprint plots[16] were obtained using CrystalExplorer 3.1.[17] As the structure of **1** contains four independent molecules in the asymmetric unit, four different Hirshfeld surfaces were obtained for **1-I**, **1-II**, **1-III** and **1-IV**.

According to the Hirshfeld surface analysis, for all molecules of **1** as well as for **2**, the intermolecular H···H contacts, comprising from 52.1 to 55.6% (Fig. 3) of the total number of contacts, are highly dominant contributors to the crystal packing. The shortest H···H contacts are shown in the fingerprint plots as characteristic spikes at $d_e + d_i \approx$ 2.2–2.3 Å (Fig. 3). A subtle feature is evident in the fingerprint plots of **1-III**, **1-IV** and **2** and less visible in the corresponding plot of **1-II** where in each of these cases a distinct splitting of the short H···H fingerprint is observed. This splitting occurs when the shortest contact is between three atoms, rather than a direct two-atom contact.[16]

The structures of all molecules of **1** and **2** are also dominated by H···C contacts, comprising from 27.4 to 31.3% (Fig. 3)

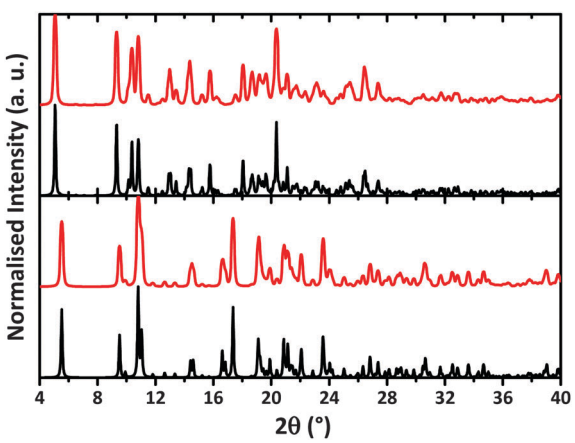

Fig. 2 Calculated (black) and experimental (red) X-ray powder diffraction patterns of **1** (top) and **2** (bottom).

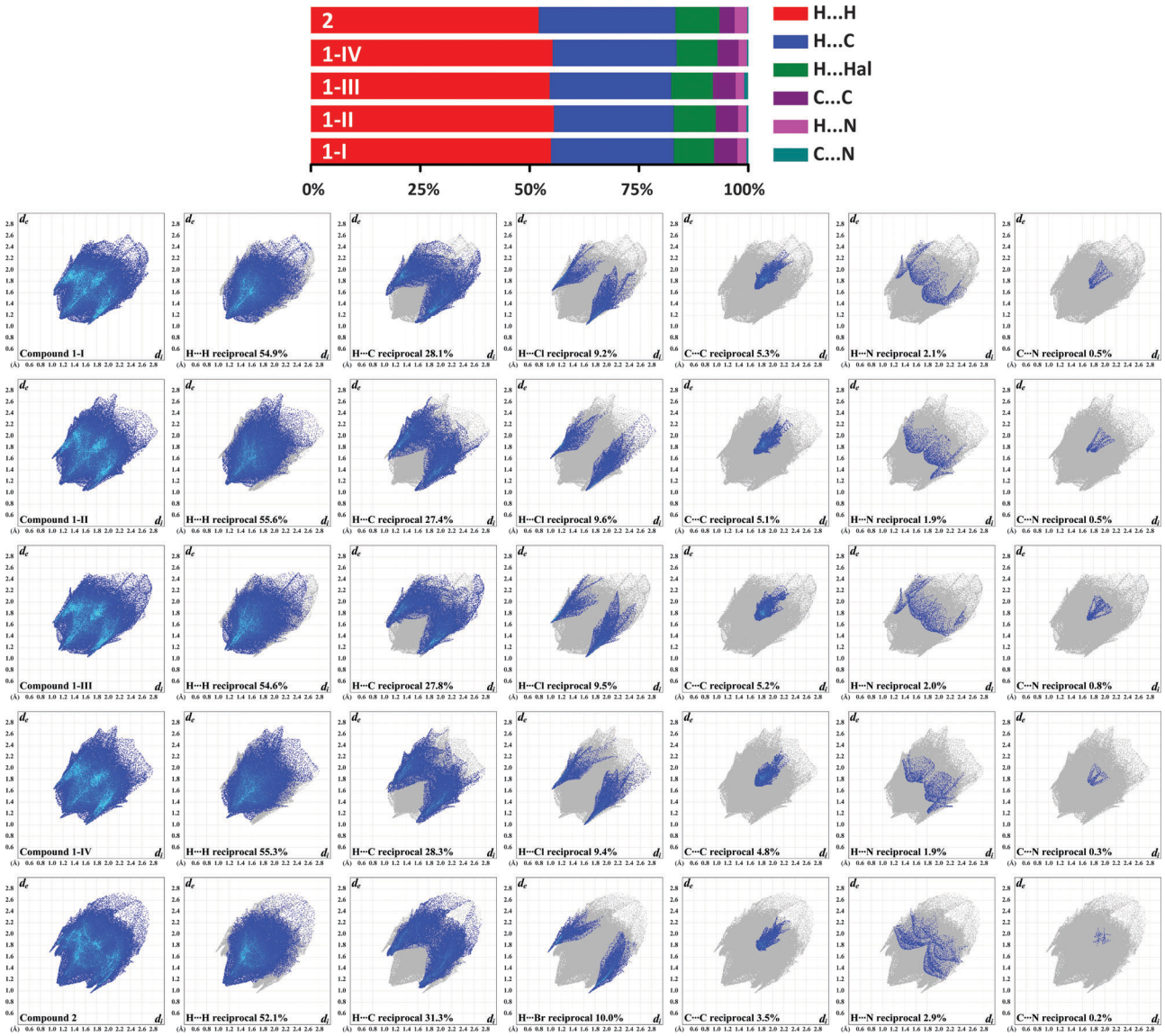

Fig. 3 Relative contributions of intermolecular contacts to the Hirshfeld surface area in **1-I**, **1-II**, **1-III**, **1-IV** and **2** (top). 2D and decomposed 2D fingerprint plots of observed contacts for **1-I**, **1-II**, **1-III**, **1-IV** and **2** (bottom).

of the total Hirshfeld surface areas. These contacts in the corresponding fingerprint plots are shown in the form of "wings" with the shortest $d_e + d_i \approx 2.6$–2.7 Å (Fig. 3), which are recognized as the characteristic of a C–H···π interaction.[16] All plots contain one more C–H···π interaction and, as a result, the overall "sawtooth" shape on the upper left and lower right of the plots is observed (Fig. 3). It is worth adding that the fingerprint plots of all molecules of **1** and **2** each exhibit a significant number of points at large d_e and d_i, shown as tails at the top right of the plots (Fig. 3). These points, similar to those observed in the fingerprint plot of benzene[16] and phenyl-containing compounds,[22] correspond to regions on the Hirshfeld surface without any close contacts to nuclei in adjacent molecules.

The structures are further characterized by a significant proportion of H···Cl in **1-I**, **1-II**, **1-III** and **1-IV** or H···Br in **2** contacts, comprising from 9.2 to 10.0% of the molecular surface (Fig. 3). The shortest H···Hal contacts are shown on the fingerprint plots as a pair of spikes at $d_e + d_i \approx 2.6$–2.7 Å (Fig. 3). Also worth mentioning is the contribution of C···C contacts ranging from 3.5 to 5.3% (Fig. 3) in both structures. They are shown on the fingerprint plots as areas on the diagonal at $d_e = d_i \approx 1.7$–2.2 Å (Fig. 3). These contacts correspond to the presence of the above-mentioned π···π stacking interactions in the crystal structures.

Close inspection of the other intermolecular contacts also revealed a negligible proportion of H···N (1.9–2.9%) and C···N (0.2–0.8%) contacts in the structures of all molecules of **1** and **2** (Fig. 3). No other contacts were found in the structures.

We have also determined the enrichment ratios (E)[18] of the intermolecular contacts for all molecules of **1** and **2** to study the propensity of two chemical species to be in contact. The enrichment ratio, derived from the Hirshfeld surface analysis,[15,17]

Table 3 Hirshfeld contact surfaces and derived "random contacts" and "enrichment ratios" for **1-I**, **1-II**, **1-III**, **1-IV** and **2**

	1-I				**1-II**				**1-III**				**1-IV**				**2**			
	H	C	N	Cl	H	C	N	Cl	H	C	N	Cl	H	C	N	Cl	H	C	N	Br
Contacts (C, %)[a]																				
H	54.9	—	—	—	55.6	—	—	—	54.6	—	—	—	55.3	—	—	—	52.1	—	—	—
C	28.1	5.3	—	—	27.4	5.1	—	—	27.8	5.2	—	—	28.3	4.8	—	—	31.3	3.5	—	—
N	2.1	0.5	0.0	—	1.9	0.5	0.0	—	2.0	0.8	0.0	—	1.9	0.3	0.0	—	2.9	0.2	0.0	—
Cl/Br	9.2	0.0	0.0	0.0	9.6	0.0	0.0	0.0	9.5	0.0	0.0	0.0	9.4	0.0	0.0	0.0	10.0	0.0	0.0	0.0
Surface (S, %)																				
	74.6	19.6	1.3	4.6	75.1	19.1	1.2	4.8	74.3	19.5	1.4	4.8	75.1	19.1	1.1	4.7	74.2	19.3	1.6	5.0
Random contacts (R, %)																				
H	55.7	—	—	—	56.4	—	—	—	55.2	—	—	—	56.4	—	—	—	55.1	—	—	—
C	29.2	3.8	—	—	28.7	3.6	—	—	29.0	3.8	—	—	28.7	3.6	—	—	28.6	3.7	—	—
N	1.9	0.1	0.0	—	1.8	0.1	0.0	—	2.1	0.1	0.0	—	1.7	0.1	0.0	—	2.4	0.1	0.0	—
Cl/Br	6.9	1.8	0.1	0.2	7.2	1.8	0.1	0.2	7.1	1.9	0.1	0.2	7.1	1.8	0.1	0.2	7.4	1.9	0.2	0.3
Enrichment (E)[b]																				
H	0.99	—	—	—	0.99	—	—	—	0.99	—	—	—	0.98	—	—	—	0.95	—	—	—
C	0.96	1.39	—	—	0.95	1.42	—	—	0.96	1.37	—	—	0.99	1.33	—	—	1.09	0.95	—	—
N	1.11	—	—	—	1.06	—	—	—	0.95	—	—	—	1.12	—	—	—	1.21	—	—	—
Cl/Br	1.33	0.00	—	—	1.33	0.00	—	—	1.34	0.00	—	—	1.32	0.00	—	—	1.35	0.00	—	—

[a] Values are obtained using CrystalExplorer 3.1.[17] [b] The "enrichment ratios" were not computed when the "random contacts" were lower than 0.9%, as they are not meaningful.[18]

is defined as the ratio between the proportion of actual contacts in the crystal and the theoretical proportion of random contacts. E is larger than unity for pairs of elements with a higher propensity to form contacts, while pairs which tend to avoid contacts yield an E value lower than unity.

The H···H and H···C contacts are favoured in the structures of all molecules of **1** and **2** since the enrichment ratios E_{HH} and E_{HC} are close to unity (0.95–1.09) and are responsible for an overwhelming majority of contacts of the interaction surface (52.1–55.6% for H···H contacts and 27.4–31.3% for H···C contacts) (Table 3). The same is observed for H···N, H···Hal and C···C contacts, which show an increased propensity to form (E_{HN} = 0.95–1.21, E_{HHal} = 1.32–1.35, E_{CC} = 0.95–1.42). This is due to relatively low values of random contacts R_{HN}, R_{HHal} and R_{CC} compared to their corresponding proportions on the total Hirshfeld surface area (Table 3).

As in the emission spectrum of [CuL(PPh$_3$)I],[13] the fluorescence spectra of **1** and **2** at 298 K show two bands upon excitation at λ_{exc} = 360 nm. The high-energy band is centred at about 420 nm in the spectra of both complexes, while the low-energy band is at 596 and 610 nm for **1** and **2**, respectively. The high-energy emission is due to the fluorescence emission from a ligand-centred $\pi \rightarrow \pi^*$ transition of **L**,[13] while the latter red-shifted emission bands, which can be isolated upon excitation with visible light at λ_{exc} = 500 nm (Fig. 4), are assigned to the mixed (M + Hal)LCT excited state.[13] The observed blue-shifting of the emission maxima of **1** and **2** compared to that of [CuL(PPh$_3$)I][13] can be explained by the replacement of the iodide by a weaker electron-donating chloride and bromide, respectively, lowering the HOMO energy level, less influencing the LUMO energy, and thus resulting in an increase of the HOMO–LUMO energy gap. This is further supported by comparison with the recently reported emission maxima at 630 and

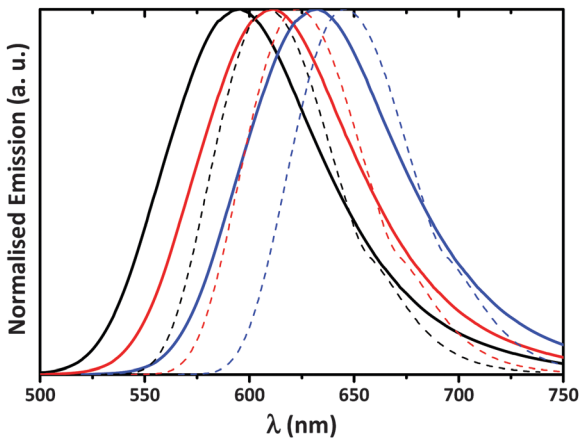

Fig. 4 Normalised solid-state emission (λ_{exc} = 500 nm) spectra of **1** (black), **2** (red) and [CuL(PPh$_3$)I][13] (blue) at 298 K (solid line) and 77 K (dashed line).

575 nm of [CuL(PPh$_3$)I] and [CuL(PPh$_3$)$_2$]BF$_4$, respectively.[13] The emission maxima of **1**, **2** and [CuL(PPh$_3$)I] are slightly (12–16 nm) shifted to longer wavelengths when the temperature was lowered to 77 K (Fig. 4). All observed emission spectra at both 298 and 77 K are broad without any vibrational features.

Conclusions

In summary, we have synthesised two mononuclear heteroleptic copper(I) complexes, [CuL(PPh$_3$)Cl] (**1**) and [CuL(PPh$_3$)Br] (**2**), with 5-phenyl-2,2′-bipyridine (**L**) and PPh$_3$, using two different metal sources, namely CuCl and CuBr, respectively. According to single crystal X-ray diffraction, both complexes are discrete neutral molecules, each revealing a tetracoordinated copper(I)

atom, which is linked to the two nitrogen atoms of **L**, one halogen and one PPh_3 with the formation of a slightly distorted trigonal pyramidal coordination core. Complex **1** displays four symmetry-independent molecules in the asymmetric unit, which can be explained through additional stabilization of the structure through cycling the chirality of the triphenylphosphine and the Cu atom through all possible enantiomers and diastereomers, and thus interleaving the triphenylphosphine groups in a double layer on the one hand, and ligand **L** and the chlorine atom in another double layer on the other hand. Both structures are additionally stabilized by weak intermolecular $\pi\cdots\pi$ stacking interactions formed between the terminal pyridine fragments of two ligands **L** corresponding to two adjacent molecules.

Hirshfeld surface analysis showed that the structures of both complexes are highly dominated by H···H and H···C contacts and also characterized by H···Hal, C···C, H···N and C···N contacts.

Both **1** and **2** were found to be emissive in the solid state, with the maxima at 596 and 610 nm, respectively, due to a (M + Hal)LCT excited state. The observed blue-shifting of the emission maximum of **1** can be explained by the replacement of the bromide by a weaker electron-donating chloride, lowering the HOMO energy level, less influencing the LUMO energy, and thus resulting in an increase of the HOMO–LUMO energy gap.

Experimental

Physical measurements

NMR spectra in DMSO-d_6 were obtained on a Bruker Avance 300 MHz spectrometer at 25 °C. ^{1}H and $^{31}P\{^1H\}$ NMR spectra were recorded at 299.948 and 121.420 MHz, respectively. Chemical shifts are reported with reference to $SiMe_4$ (^{1}H) and 85% H_3PO_4 ($^{31}P\{^1H\}$). Solid-state emission spectra were obtained using a Fluorolog-3 (Jobin-Yvon-Spex Company) spectrometer. All emissions spectra were normalized to allow meaningful comparisons. Elemental analyses were performed on a Thermoquest Flash EA 1112 Analyzer from CE Instruments.

Hirshfeld surface analysis

The Hirshfeld molecular surfaces[15] and their associated 2D fingerprint plots[16] were generated using the CrystalExplorer 3.1 software[17] from the crystal structures. The d_{norm} (normalized contact distance) surface and the breakdown of the 2D fingerprint plots were used for decoding and quantifying the intermolecular interactions in the crystal lattice. The d_{norm} is a symmetric function of distances to the surface from the nuclei inside (d_i) and outside (d_e) the Hirshfeld surface, relative to their respective van der Waals radii. 2D fingerprint plots were generated using d_i and d_e in the translated 0.4–3.0 Å range and including reciprocal contacts as a pair of coordinates in 2D histograms. A color gradient in the fingerprint plots ranging from blue to red is used to visualize the proportional contribution of contact pairs to the global surface.

Enrichment ratio

The enrichment ratio (E)[18] of a pair of elements (X,Y) is the ratio between the proportion of actual contacts in the crystal and the theoretical proportion of random contacts. E is larger than unity for pairs of elements which have a high propensity to form contacts in crystals, while pairs which tend to avoid contacts with each other yield an E value lower than unity. E values are calculated from the percentage of contacts, which, in turn, are given by the CrystalExplorer 3.1 software,[17] between one type or two types of chemical elements in a crystal packing.

Synthesis of 1 and 2

A solution of **L** (0.1 mmol, 23.2 mg) in CH_2Cl_2 was added dropwise under vigorous stirring to a mixture of CuCl or CuBr (0.1 mmol; 10.0 and 14.3 mg, respectively) and PPh_3 (0.2 mmol, 52.5 mg) in the same solvent (10 mL). The mixture was stirred at room temperature for 1 h. The solvent was then removed *in vacuo*. Complexes were isolated by recrystallisation from a 1 : 4 mixture of CH_2Cl_2 and *n*-hexane.

1. Orange crystals. Yield: 49.9 mg (84%). ^{1}H NMR, δ: 7.26–7.42 (m, 6H, *o*-H, PPh_3), 7.45–7.81 (m, 15H, *m*-H + *p*-H, PPh_3; L), 7.97–9.08 (br. s, 5H, L), 10.51–11.47 (br. s, 2H, L) ppm. $^{31}P\{^1H\}$ NMR, δ: 25.8 (s) ppm. Anal. calc. for $C_{34}H_{27}ClCuN_2P$ (593.57): C 68.80, H 4.58, N 4.72. Found: 68.72, 4.64, N 4.78%.

2. Orange crystals. Yield: 58.7 mg (92%). ^{1}H NMR, δ: 7.30–7.52 (m, 6H, *o*-H, PPh_3), 7.51–7.75 (m, 15H, *m*-H + *p*-H, PPh_3; L), 8.09–9.13 (br. s, 5H, L), 10.69–11.58 (br. s, 2H, L) ppm. $^{31}P\{^1H\}$ NMR, δ: 25.9 (s) ppm. Anal. calc. for $C_{34}H_{27}BrCuN_2P$ (638.03): C 64.01, H 4.27, N 4.39. Found: 63.90, 4.21, N 4.46%.

X-Ray powder diffraction

X-Ray powder diffraction of bulk samples was carried out using a MAR345 diffractometer equipped with a rotating anode (MoKα radiation) and a XENOCS focusing mirror.

Single-crystal X-ray diffraction study

The X-ray data for **1** and **2** were collected at 150(2) K on a Mar345 image plate detector using MoKα radiation (Xenocs Fox3D mirror). The data were integrated with the CrysAlis(Pro) software.[23] The implemented empirical absorption correction was applied. The structures of **1** and **2** were solved by SHELXS[24] and refined by full-matrix least squares on $|F^2|$, using SHELXL2014/7.[25] Non-hydrogen atoms were anisotropically refined and the hydrogen atoms were placed on calculated positions in riding mode with temperature factors fixed at 1.2 times U_{eq} of the parent atoms. For **1** the measured crystal was found to be twinned and the TWINROTMAT procedure in PLATON[26] was used to deconvolute the two twin domains. Figures were generated using the program Mercury.[27]

Crystal data for 1. $C_{34}H_{27}ClCuN_2P$, M_r = 593.53 g mol^{-1}, triclinic, space group $P\bar{1}$, a = 16.837(2) Å, b = 19.0230(16) Å, c = 19.862(3) Å, α = 115.622(11)°, β = 101.572(12)°, γ = 90.310(9)°, V = 5588.7(13) Å^3, Z = 8, ρ = 1.411 g cm^{-3}, μ(Mo-Kα) = 0.961 mm^{-1}, reflections: 18 953 collected, 18 953 unique, R_{int} = 0.000, R_1(all) = 0.0746, wR_2(all) = 0.1435.

Crystal data for 2. $C_{34}H_{27}BrCuN_2P$, M_r = 637.99 g mol^{-1}, orthorhombic, space group *Pbca*, a = 9.5272(3) Å, b = 18.5794(6) Å, c = 32.0159(14) Å, V = 5667.1(4) Å^3, Z = 8, ρ = 1.496 g cm^{-3}, μ(Mo-Kα) = 2.264 mm^{-1}, reflections: 32 759 collected, 5112 unique, R_{int} = 0.085, R_1(all) = 0.0604, wR_2(all) = 0.0827.

Acknowledgements

We thank WBI (Belgium) for post-doctoral positions allocated to D. A. Safin and M. G. Babashkina.

References

1 (*a*) F. A. Cotton and G. Wilkinson, *Advanced Inorganic Chemistry*, Wiley, New York, 1980; (*b*) K. Kalyanasundaram, *Photochemistry of Polypyridine and Porphyrin Complexes*, Academic Press, London, 1992; (*c*) A. P. de Silva, D. B. Fox, A. J. M. Huxley and T. S. Moody, *Coord. Chem. Rev.*, 2000, **205**, 41; (*d*) C. Bargossi, M. C. Fiorini, M. Montalti, L. Prodi and N. Zaccheroni, *Coord. Chem. Rev.*, 2000, **208**, 17; (*e*) A. Vogler and H. Kunkely, *Top. Curr. Chem.*, 2001, **213**, 143; (*f*) T. G. Drummond, M. G. Hill and J. K. Barton, *Nat. Biotechnol.*, 2003, **21**, 1192; (*g*) V. Balzani and C. Campagna, *Photochemistry and Photophysics of Coordination Compounds I*, Springer, Berlin, 2007; (*h*) V. Balzani and C. Campagna, *Photochemistry and Photophysics of Coordination Compounds II*, Springer, Berlin, 2007; (*i*) M. K. Nazeeruddin and M. Grätzel, *Struct. Bonding*, Springer, Berlin, 2007, vol. 123, p. 113.

2 (*a*) D. R. McMillin and K. M. McNett, *Chem. Rev.*, 1998, **98**, 1201; (*b*) P. C. Ford, E. Cariati and J. Bourassa, *Chem. Rev.*, 1999, **99**, 3625; (*c*) N. Armaroli, G. Accorsi, F. Cardinali and A. Listorti, *Top. Curr. Chem.*, 2007, **280**, 69; (*d*) Z. Liu, W. He and Z. Guo, *Chem. Soc. Rev.*, 2013, **42**, 1568; (*e*) Z. Liu, W. Qi and G. Xu, *Chem. Soc. Rev.*, 2015, **44**, 3117.

3 (*a*) V. W. W. Yam and K. K. W. Lo, *Chem. Soc. Rev.*, 1999, **28**, 323; (*b*) Q. Zhang, Q. Zhou, Y. Cheng, L. Wang, D. Ma, X. Jing and F. Wang, *Adv. Mater.*, 2004, **16**, 432; (*c*) N. Armaroli, G. Accorsi, M. Holler, O. Moudam, J.-F. Nierengarten, Z. Zhou, R. T. Wegh and R. Welter, *Adv. Mater.*, 2006, **18**, 1313; (*d*) M. Nishikawa, K. Nomoto, S. Kume, K. Inoue, M. Sakai, M. Fujii and H. Nishihara, *J. Am. Chem. Soc.*, 2010, **132**, 9579.

4 (*a*) D. G. Cuttell, S. M. Kuang, P. E. Fanwick, D. R. McMillin and R. A. Walton, *J. Am. Chem. Soc.*, 2002, **124**, 6; (*b*) M. G. Babashkina, D. A. Safin, M. Bolte and A. Klein, *CrystEngComm*, 2009, **12**, 134; (*c*) C. S. Smith, C. W. Branham, B. J. Marquardt and K. R. Mann, *J. Am. Chem. Soc.*, 2010, **132**, 14079; (*d*) D. A. Safin, M. G. Babashkina, M. Bolte and A. Klein, *Inorg. Chim. Acta*, 2010, **363**, 1897; (*e*) M. G. Babashkina, D. A. Safin, A. Klein and M. Bolte, *Eur. J. Inorg. Chem.*, 2010, 4018; (*f*) D. A. Safin, M. G. Babashkina and A. Klein, *Croat. Chem. Acta*, 2010, **83**, 353; (*g*) D. A. Safin, M. G. Babashkina, M. Bolte and A. Klein, *CrystEngComm*, 2011, **13**, 568; (*h*) D. A. Safin, M. G. Babashkina, M. Bolte and M. Köckerling, *Inorg. Chim. Acta*, 2011, **370**, 59; (*i*) M. G. Babashkina, D. A. Safin and Y. Garcia, *Polyhedron*, 2012, **33**, 114.

5 C. E. Housecroft and E. C. Constable, *Chem. Soc. Rev.*, 2015, **44**, 8386.

6 D. A. Safin, J. Frost and M. Murugesu, *Dalton Trans.*, 2015, **44**, 20287.

7 F. H. Case and E. Koft, *J. Am. Chem. Soc.*, 1959, **81**, 905.

8 (*a*) E. I. Lerner and S. J. Lippard, *Inorg. Chem.*, 1977, **16**, 1537; (*b*) A. M. Garcia, D. M. Bassani, J.-M. Lehn, G. Baum and D. Fenske, *Chem. – Eur. J.*, 1999, **5**, 1234.

9 (*a*) D. A. Safin, Y. Xu, I. Korobkov, D. L. Bryce and M. Murugesu, *CrystEngComm*, 2013, **15**, 10419; (*b*) D. A. Safin, N. A. Tumanov, A. A. Leitch, J. L. Brusso, Y. Filinchuk and M. Murugesu, *CrystEngComm*, 2015, **17**, 2190; (*c*) D. A. Safin, K. M. N. Burgess, I. Korobkov, D. L. Bryce and M. Murugesu, *CrystEngComm*, 2014, **14**, 3466; (*d*) D. A. Safin, R. J. Holmberg, K. M. N. Burgess, K. Robeyns, D. L. Bryce and M. Murugesu, *Eur. J. Inorg. Chem.*, 2015, 441; (*e*) D. A. Safin, A. Pialat, I. Korobkov and M. Murugesu, *Chem. – Eur. J.*, 2015, **21**, 6144; (*f*) D. A. Safin, A. Pialat, A. A. Leitch, N. A. Tumanov, I. Korobkov, Y. Filinchuk, J. L. Brusso and M. Murugesu, *Chem. Commun.*, 2015, **51**, 9547; (*g*) D. A. Safin, P. M. J. Szell, A. Keller, I. Korobkov, D. L. Bryce and M. Murugesu, *New J. Chem.*, 2015, **39**, 7147.

10 (*a*) J. Kotlicka and Z. R. Grabowski, *J. Photochem.*, 1979, 413; (*b*) G. Albano, V. Balzani, E. C. Constable, M. Maestri and D. R. Smith, *Inorg. Chim. Acta*, 1998, **277**, 225.

11 B. Bosnich, *Acc. Chem. Res.*, 1969, **2**, 266.

12 J. C. Loren and J. S. Siegel, *Angew. Chem., Int. Ed.*, 2001, **40**, 754.

13 D. A. Safin, M. P. Mitoraj, K. Robeyns, Y. Filinchuk and C. M. L. Vande Velde, *Dalton Trans.*, 2015, **44**, 16824.

14 (*a*) V. N. Kozhevnikov, D. N. Kozhevnikov, O. V. Shabunina, V. L. Rusinov and O. N. Chupakhin, *Tetrahedron Lett.*, 2005, **46**, 1791; (*b*) D. N. Kozhevnikov, O. V. Shabunina, D. S. Kopchuk, P. A. Slepukhin and V. N. Kozhevnikov, *Tetrahedron Lett.*, 2006, **47**, 7025.

15 M. A. Spackman and D. Jayatilaka, *CrystEngComm*, 2009, **11**, 19.

16 M. A. Spackman and J. J. McKinnon, *CrystEngComm*, 2002, **4**, 378.

17 S. K. Wolff, D. J. Grimwood, J. J. McKinnon, M. J. Turner, D. Jayatilaka and M. A. Spackman, *CrystalExplorer 3.1*, University of Western Australia, 2012.

18 C. Jelsch, K. Ejsmont and L. Huder, *IUCrJ*, 2014, **1**, 119.

19 L. Yang, D. R. Powell and R. P. Houser, *Dalton Trans.*, 2007, 955.

20 (*a*) W. Yao, O. Eisenstein and R. H. Crabtree, *Inorg. Chim. Acta*, 1997, **254**, 105; (*b*) Y. Zhang, J. C. Lewis, R. G. Bergman, J. A. Ellman and E. Oldfield, *Organometallics*, 2006, **25**, 3515; (*c*) M. Brookhart, M. L. H. Green and G. Parkin, *Proc. Natl. Acad. Sci. U. S. A.*, 2007, **104**, 6908; (*d*) H. V. Huynh, L. R. Wong and P. S. Ng, *Organometallics*, 2008, **27**, 2231; (*e*) J. Saßmannshausen, *Dalton Trans.*, 2012, **41**, 1919; (*f*) K. A. Siddiqui and E. R. T. Tiekink, *Chem. Commun.*, 2013, **49**, 8501; (*g*) S. Schöler, M. H. Wahl, N. I. C. Wurster, A. Puls, C. Hättig and G. Dyker, *Chem. Commun.*, 2014,

50, 5909; (*h*) M. G. D. Holaday, G. Tarafdar, A. Kumar, M. L. P. Reddy and A. Srinivasan, *Dalton Trans.*, 2014, **43**, 7699; (*i*) W. Scherer, A. C. Dunbar, J. E. Barquera-Lozada, D. Schmitz, G. Eickerling, D. Kratzert, D. Stalke, A. Lanza, P. Macchi, N. P. M. Casati, J. Ebad-Allah and C. Kuntscher, *Angew. Chem., Int. Ed.*, 2015, **54**, 2505.

21 T. Steiner, *Angew. Chem., Int. Ed.*, 2002, **41**, 48.

22 For example: (*a*) D. A. Safin, M. P. Mitoraj, K. Robeyns, Y. Filinchuk and C. M. L. Vande Velde, *Dalton Trans.*, 2015, **44**, 16824; (*b*) M. G. Babashkina, K. Robeyns, Y. Filinchuk and D. A. Safin, *New J. Chem.*, 2016, **40**, 1230.

23 *Rigaku Oxford Diffraction, CrysAlis(Pro) Software system, version 1.171.37.31*, Rigaku Corporation, Oxford, UK, 2014.

24 G. M. Sheldrick, *Acta Crystallogr., Sect. A: Found. Crystallogr.*, 2008, **64**, 112.

25 G. M. Sheldrick, *SHELXL2014/7*, University of Göttingen, Germany, 2014.

26 A. L. Spek, *Acta Crystallogr., Sect. D: Biol. Crystallogr.*, 2009, **65**, 148.

27 I. J. Bruno, J. C. Cole, P. R. Edgington, M. Kessler, C. F. Macrae, P. McCabe, J. Pearson and R. Taylor, *Acta Crystallogr., Sect. B: Struct. Sci.*, 2002, **58**, 389.

